INTERNATIONAL CONFERENCE ON LIGHTNING PROTECTION
33rd International Conference on Lightning Protection
25 - 30 September 2016
Estoril, Portugal

Varistor Coupling for Combination Wave Test of Surge Protective Devices

Jianguo Wang, Mi Zhou, Yadong Fan, Li Cai, Lixian Pei, and Quanxin Li
School of Electrical Engineering, Wuhan University
Wuhan, China
wjg@whu.edu.cn, zhoumi927@whu.edu.cn, ydfan@whu.edu.cn, caili@ whu.edu.cn, plx@whu.edu.cn, quanxinli@whu.edu.cn

***Abstract*—The waveform influencing characteristics by vasistor coupling of combination wave test waveforms of surge protective devices (SPD) is studied in this paper. EPCOS vavistors, with maximum operating voltages ranging between 130 V and 750 V, are adopted here in OrCAD/Pspice environment to analyze the influence of vavistor coupling on output characteristic of the combination wave generator in test levels of 0 to 20 kV. Obtained results show that, owing to the varistor coupling, reverse oscillation phenomena will arise in the open-circuit voltages. The peak value, the front time, and the tail time of both open-circuit voltage and short-circuit current will decrease, whereas the virtual impedance will increase. The lower the test level, or the higher the maximum operating voltage of the vavistor, the more serious this effect. Compared with the conventional capacitor coupling, the range of the voltage of power supply networks and the levels of combination wave test by varistor coupling have to be limited to a great extent. Varistor coupling for combination wave test of SPD should be only used in special cases and special test levels where there are no strict waveforms limitations.**

Keywords- Combination wave; coupling network; OrCAD/PSpice; surge protective device (SPD); vavistor.

I. INTRODUCTION

In powered testing of class III surge protective device (SPD), the surges need to be applied to the test sample through the coupling network, in order to limit the steady-state, power-frequency current flow drained from the power line into the combination wave generator (CWG). Decoupling network is used, on one hand, to provide sufficient impedance for the test surge, and on the other hand, to prevent the surge from being fed back to the power-supply network [1]–[5].

In the case of powered testing of SPD where the coupling/decoupling network is involved, the coupling network will, however, become a part of load of CWG, resulting in inevitable alteration of the output waveforms of the CWG. In the presence of coupling/decoupling network, the output waveforms, including the amplitude, the duration time, as well as the undershoot of 1.2/50-μs open-circuit voltage (OCV) and of 8/20-μs short-circuit current (SCC), of the CWG should be verified at the terminals of the test sample. The virtual impedance (VI), defined as the ratio of peak OCV to peak SCC, is another important parameter to be considered. Table I gives, for various relevant standards [6]–[8], a summary and comparison of the specifications for OCV, SCC, and VI measured at the output port of CWG in this case.

Capacitive coupling is recommended in [6]–[8] and is addressed in detail by Zhou *et al.* [5], who reported that there is a compromise between having a large enough coupling capacitance to yield more normalized OCV and SCC waveforms, and a low coupling capacitance which is able to limit the steady-state current flow into the CWG. Due to this defect, broader tolerances of surge waveforms were recommended by Zhou *et al.* [5] to IEC 61643-1 [9], a former edition of IEC 61643-11 [6], after the coupling/decoupling network is connected to CWG (see Tables V and VI in [5]).

Metal oxide varistor (MOV), which presents high impedance under power-frequency conditions and low impedance for the surge, have an operating current of the order of microamperes. MOVs have the advantage that they can operate in nanoseconds or less, and that they can be constructed to conduct relatively large current, up to tens of thousands of amperes [10]. Perhaps due to the concern about the problem of power-frequency current flow in capacitor coupling, ITU-T K.44 [11] suggests the use of MOVs as coupling elements since they can limit the flow of power-frequency current from the power line into the CWG. Nevertheless, unlike the capacitor that is linear, MOVs are basically non-linear resistors, probably making them problematic since the response characteristics of MOV might be different under various test levels. Until now, it appears that very few efforts have been devoted to the application feasibility of MOV coupling.

Following the above discussion, in this study, we analyze the influence of MOV coupling on OCV, SCC, and VI generated by the CWG in the presence of coupling/decoupling network. The paper is organized as follows. In Section II, we present the circuit model of a CWG with a single-phase coupling/decoupling network connected, in which the MOV serves as the coupling element. In that section, the varistor model in OrCAD/PSpice environment is described in detail. Valid test levels by varistor coupling are recommended to IEC 61643-11 and to UL 1449. Influence of varistor coupling on the OCV, SCC, and VI is simulated in Section III. Section III is also dedicated to the decoupling effect in the case of varistor coupling, as well as a comparison with that of capacitor coupling. Discussions and conclusions are given in Sections IV and V, respectively.

This work was supported by National Natural Science Foundation of China (Grant number: 51207116).

TABLE I. WAVEFORMS SPECIFICATIONS AT THE EQUIPMENT PORT OF COUPLING/DECOUPLING NETWORK IN VARIOUS STANDARDS

Standard	Open-circuit voltage			Short-circuit current			Fictive impedance (Ω)
	Front time (μs)	Tail time (μs)	Undershoot	Front time (μs)	Tail time (μs)	Undershoot	
IEC 61643-11:2011	0.84~1.56	40~60	<20 %	7.2~8.8	18~22	<20 %	1.8~2.2
UL 1449:2009	0.84~1.56	40~60	Not required	6.5~9.0	16~28	Not required	1.5~2.5
IEC 61000-4-5:2014	0.84~1.56	Current rating≤16A: 40~60; 16A<Current rating ≤32A: 35~60; 32A<Current rating ≤63A: 30~60; 63A<Current rating ≤125A: 25~60; 125A<Current rating ≤200A: 20~60	Not required	6.4~9.6	16~24	Not required	Not required

II. ANALYSIS MODEL AND PARAMETERS

Six types of EPCOS varistors, namely, LS40K130QP, LS40K230QP, LS40K320QP, LS40K420QP, LS40K550QP, and LS40K750QP, with the largest operating voltage of 130, 230, 320, 420, 550, and 750 V respectively, were used as the research objects. Our circuit model was implemented in OrCAD/Pspice program because its parametric sweep tool allows us to easily get insight into design space by sweeping a parameter within a range of values and displaying how the performance of the design changes. The other reason, the more important one to us, is that the PSpice model for MOVs are supplied by EPCOS.

Fig. 1 shows our simulation model of CWG in the presence of a single-phase coupling/decoupling network, in which the MOV serves as the coupling network. The CWG is made up of the storage capacitor C_c (8 μF) with an initial charge voltage U, switch S, and pulse shaping network consisting of R_{S1} (15 Ω), R_{S2} (25 Ω), L_r (10 μH), and R_m (1.2 Ω). These circuit parameters were determined using a trial-and-error approach to obtain a 1.15/55.51-μs OCV,7.66/21.90-μs SCC, and 2.09-Ω VI, in the absence of the coupling/decoupling network or any other components, as shown in Fig. 2. Note that, the front time of OCV is a virtual parameter defined as 1.67 times the interval between the instants when the impulse is 30% and 90% of the peak value, whereas the front time of SCC is defined as 1.25 times the interval between the instants when the impulse is 10% and 90% of the peak value. Note also that, for both OCV and SCC, although their waveshapes meet the requirement in [6]–[8], the tail times are slightly larger than the corresponding nominal value because, as reported in [5], the time durations of OCV and SCC produced by the CWG alone are preferable to be longer, for the sake of diminishing the effect of coupling/decoupling network.

Decoupling network, as essentially a low-pass filter to provide blocking capability for the surge, consists of decoupling inductors L_1, L_2 (air-core type, 1.5 mH) and decoupling capacitors C_1, C_2, and C_3 (15 μF). The component values of decoupling network, including decoupling inductance

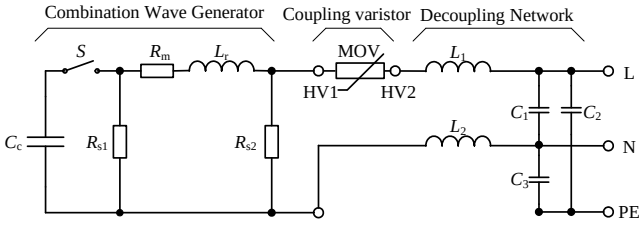

Figure 1. Simulation circuit of varistor coupling for combination wave generator.

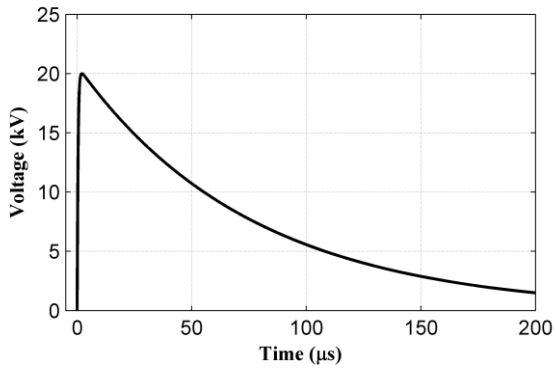

(a)

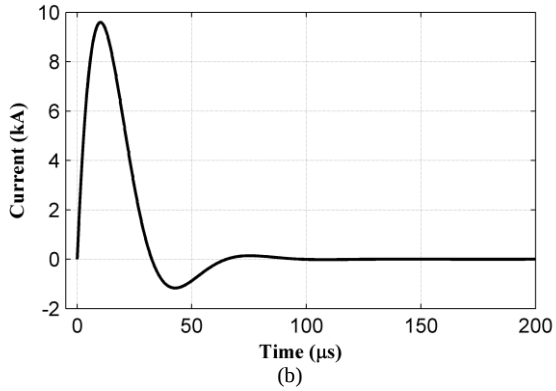

(b)

Figure 2. (a) OCV and (b) SCC waveforms produced by the simulated CWG model between terminals "HV1" and "LV" in Fig. 1, when the coupling/decoupling network is not connected.

and decoupling capacitance, were designed based on the principle that, as specified in [8], the residual surge voltage on the power supply inputs of the decoupling network when the test sample is disconnected shall not exceed 15 % of the applied test voltage or twice the rated peak voltage of the coupling/decoupling network, whichever is higher. More details can be found in [4].

The polarization phenomenon in small current region, the dynamic voltage-ampere characteristics under the effect of impulse current, and the overshoot phenomenon under the effect of steep front impulse current should be taken into consideration in the equivalent circuit of varistor models [12]-[17]. The equivalent circuit for the varistor model (see MOV in Fig. 1) in OrCAD/PSpice environment is shown in Fig. 3, where L-SERIES is the series lead inductance, R-SERIES is a given parameter for calculating to stabilize the numerical integration, and C-PAR is the parallel capacitor. The values of L-SERIES and R-SERIES are 14 nH and 100 nΩ, respectively, for all the six types of varistors. Values of C-PAR are, in order of increasing operating voltage, 5600, 3200, 2300, 1800, 1400, and 1000 pF, respectively. R-VAL is nonlinear resistor which can be simulated by the current controlled voltage source in OrCAD/PSpice. The voltage-ampere characteristics of R-VAL is characterized as

$$\log(u) = B_1 + B_2 \cdot \log(i) + B_3 \cdot \exp(-\log(i)) + B_4 \cdot \exp(-\log(i)) \quad (1)$$

where B_1, B_2, B_3, and B_4 are characteristic parameters whose values are presented in Table II, i is the current, and u is the voltage. As an example, Fig. 4 gives the response of LS40K320QP under an 8/20-μs current.

III. Analyses and Results

As aforementioned in Section I, in the case that the coupling/decoupling network is connected to the CWG, the OCV, SCC and VI should be obtained from the ports of HV2 and LV in Fig. 1, in the condition that L, N and PE are connected together to simulate the low mains impedance. The charging voltage of C_c, henceforth referred to as charging voltage, will be adjusted in the following analyses since, owing to the nonlinear property of MOV, they behave dissimilarly under different voltage levels.

A. Open-circuit Voltage

Simulations were run to obtain the OCVs coupled by the six types of EPCOS, as the charging voltage increases from 0 to 21.51 kV. Fig. 5 shows a three-dimensional view of the OCV waveforms for the case of LS40K130QP coupling. It should be mentioned that only under a certain voltage level can the varistor operate, and thus, will a surge emerge between ports of HV2 and LV.

The front time, the tail time, and the undershoot of the obtained OCV, with the evolution of charging voltage, are presented in Fig. 6. Fig. 6(b) gives, for all the six coupling elements, the computed front time of OCV. As shown in Fig. 6(b), with the increase of the charging voltage, all the front

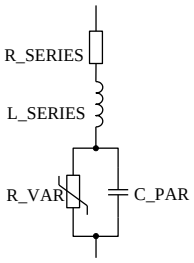

Figure 3. Equivalent circuit of the varistor.

TABLE II. PARAMETERS USED FOR THE VARISTOR MODEL

Varistor type	B_1	B_2	B_3	B_4
LS40K130QP	2.399277	0.024184	-0.000679	0.002765
LS40K230QP	2.672993	0.024459	-0.000390	0.003235
LS40K320QP	2.783471	0.023687	-0.000242	0.003471
LS40K420QP	2.907262	0.023899	-0.000162	0.003461
LS40K550QP	3.033246	0.023941	-0.000126	0.003570
LS40K750QP	3.157001	0.025082	-0.000129	0.003422

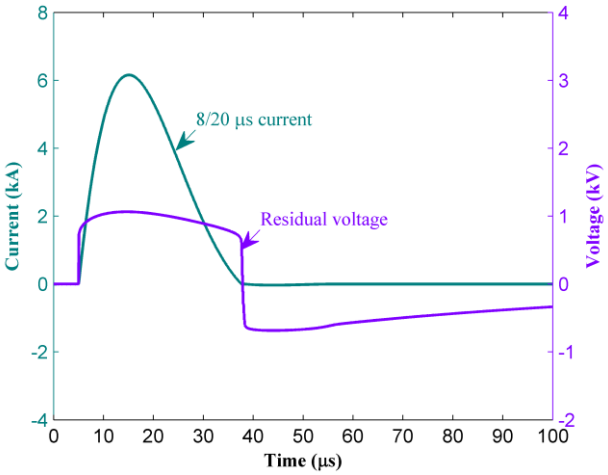

Figure 4. Response of LS40K320QP under an 8/20-μs current

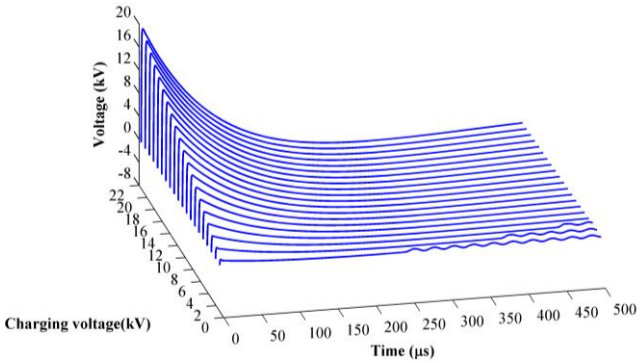

Figure 5. Waveform of OCV for LS40K130QP coupling under the condition of different charging voltages of C_c.

times initially remain constant, and then increase gradually. All the front times in Fig. 6(b) are smaller than that in the absence

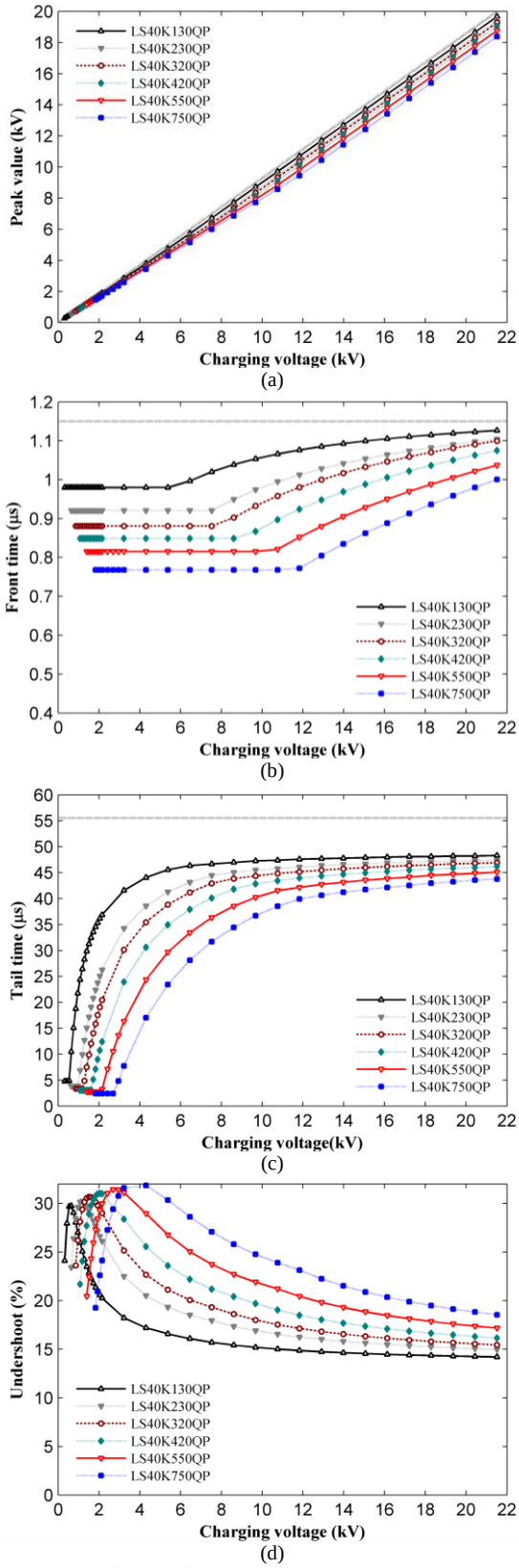

Figure 6. Influence of varistor coupling on open-circuit voltage waveforms, under the condition of different charging voltages of Cc. (a) peak value, (b) front time, (c) tail time, (d) undershoot of six varistors' coupling.

of coupling/decoupling network. For LS40K550QP and LS40K750QP coupling, the front times of OCV are smaller than 0.84 μs when the charging voltage is below 10.8 and 14.0 kV, respectively.

The tail time, or termed as time to half-value, of the OCVs are presented in Fig. 6(c). Contrary to those observed in the front times, the tail times firstly increase gradually, and then remain at constant values which are still smaller than the tail time of OCV in the absence of coupling/decoupling network.

For the six varistors, only in the condition that the charging voltage is, in order of increasing operating voltage, larger than 3.2, 5.2, 6.0, 7.5, 9.7, and 12.9 kV, respectively, will the tail time of OCV be larger than 40 μs, the minimum value meeting requirement of IEC 61643-11. Further, inferring from Fig. 6(b) and Fig. 6(c), both the front times and tail times of OCVs coupled by a MOV with a larger maximum continuous operating voltage will be decreased more significantly.

Oscillation phenomenon, not observed in the absence of the coupling/decoupling network, can be found in the OCV by MOV coupling. Fig. 6(d) presents the calculated results of OCV undershoot, a parameter defined as the ratio of the minus peak to the positive peak if the charging voltage is positive. The undershoot increase at first, and then decrease gradually with the increase of charging voltage. For six varistors, when the charging voltage is larger than, in order of increasing operating voltage, 2.2, 4.3, 6.5, 8.6, 11.8, and 16.2 kV, respectively, undershoot of OCV will exceed 20%, a threshold value specified in IEC 61643-11.

According to the above analysis, compared with the condition of CWG without the coupling/decoupling network connected, the peak value, the front time, and the tail time of OCV will be decreased in the condition of varistor coupling. This decreasing effect will be more obvious if the maximum operating voltage of the varistors is higher. The OCV waveforms can meet the requirements of IEC 61643-11 only when the charging voltage of C_c is larger than, in order of increasing operating voltage, 3.2, 5.2, 6.5, 8.6, 11.8, and 16.2 kV, respectively.

B. Short-circuit Current

Except that HV2 and LV should be connected, to analyze the influence of varistor coupling on the SCC waveforms, simulation settings are the same as those for OCV. Fig. 7 is SCC waveforms for LS40K130QP coupling. Due to the load effect of MOV, the peak values of SCC by varistor coupling are lower than the case that the coupling/decoupling network is connected. Again, only when the charging voltage exceeds a certain value can the varistor operate. Otherwise, there will be no current output.

Fig. 8 (b) presents the front times of SCC, showing that as the charging voltage increases, the front times increase significantly at first and then remain constant. Compared with that of SCC in Fig. 2, the front times are decreased, and the higher the maximum running voltage of varistor, the smaller the front times. For the six varistors, in the case that the charging voltage is larger than, in order of increasing operating

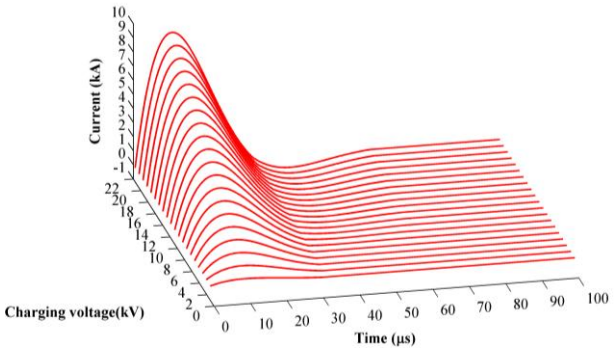

Figure 7. Waveform of SCC for LS40K130QP coupling under the condition of different charging voltages of C_c.

voltage, 1.0, 2.0, 3.2, 4.3, 6.4, 8.6 kV, respectively, the front times of SCC are larger than 7.2 μs, the minimum value in accordance with requirement of IEC 61643-11.

The tail times of SCC are presented in Fig. 8(c). Similar to the variation trend of front times with the evolution of charging voltage, the tail times also increase at first and then remain constant. In respect to undershoot, the SCC waveforms LS40K550QP or LS40K750QP coupling do not feature with oscillation phenomenon. For other four varistors with smaller maximum operating voltages, as shown in Fig. 8(d), as the charging voltages increase, no oscillations are observed at first, then oscillations emerge and the undershoot increase gradually. The lower the maximum operating voltage, the larger the undershoot. However, all the involved undershoot is below the maximum required value in IEC 61643-11, 20%.

According to the analysis above, under the condition of varistor coupling, the peak value, the front time, the tail time, and the undershoot of SCC will be decreased. For the six varistors, when the charging voltage is larger than, in order of increasing operating voltage, 1.0, 2.0, 3.2, 4.3, 6.4, 8.6 kV, respectively, the waveforms of SCC will meet the requirements of IEC61643-11.

C. Virtual Impedance

Fig. 9 presents the variation of VI as a function of charging voltage. It follows from Fig. 9 that VI has increased due to the effect of the impedance of varistor, and that the higher the maximum operating voltage of the varistor, the larger the VI. For LS40K750QP coupling, within the range of charging voltage of 0 to 21.51 kV, the VI is always larger than 2.2 Ω, the maximum limit specified in IEC 61643-11. For the remaining five varistors, if the charging voltage is, in order of increasing operating voltage, larger than 3.8, 6.5, 7.5, 10.8, and 18.3 kV, respectively, the VI is smaller than 2.2 Ω.

From the above analyses, it can be found that the higher the maximum operating voltage of varistors, the worse its coupling performance. If OCV, SCC and VI meet the requirements of IEC 61643-11 which has a relatively large test level (i.e., 20 kV/10 kA), the charging voltage of the circuit should be larger than 3.8, 6.5, 7.5, 10.8, 18.3 kV respectively for

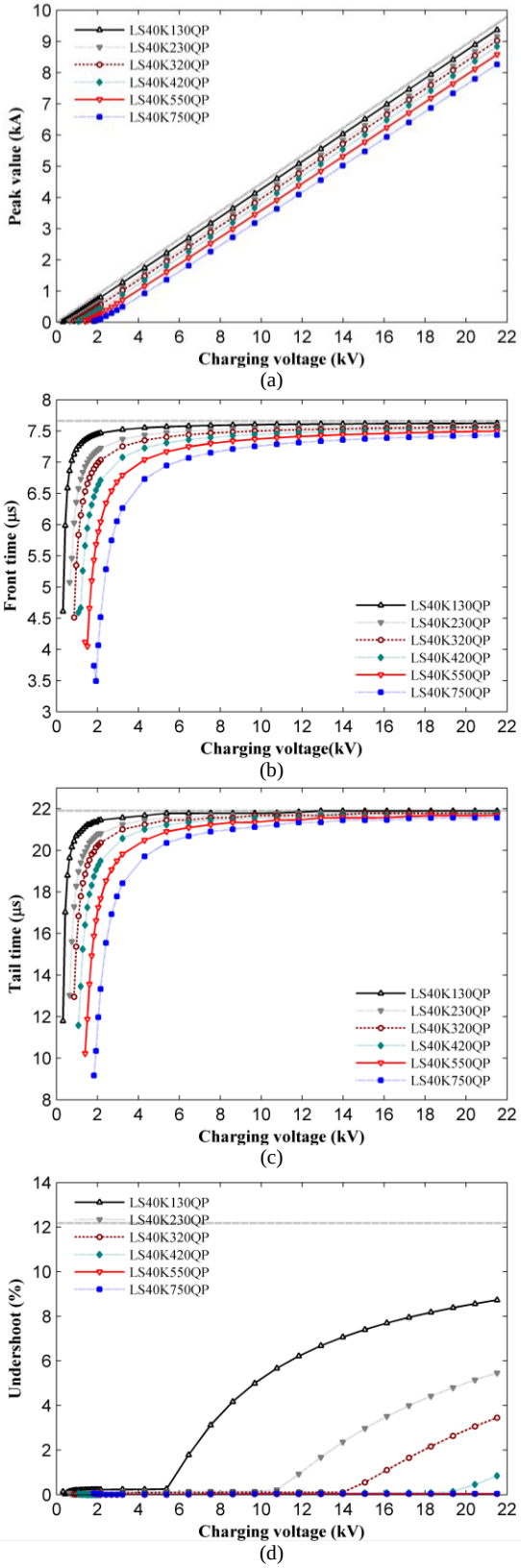

Figure 8. Influence of varistor coupling on short-circuit current waveforms, under the condition of different charging voltages of Cc. (a) peak value, (b) front time, (c) tail time, (d) undershoot of six varistors' coupling.

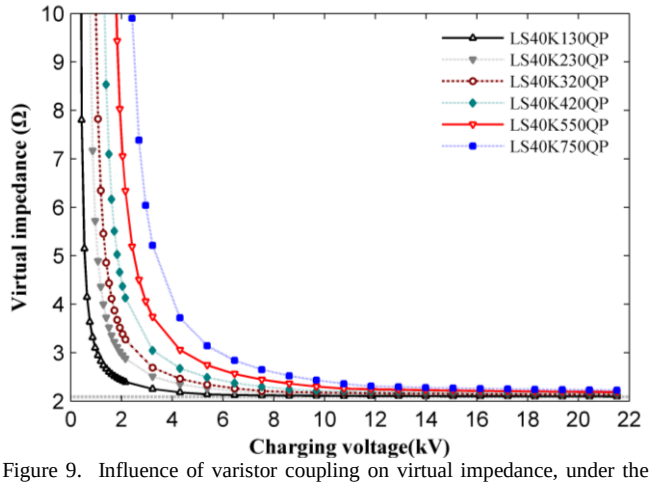

Figure 9. Influence of varistor coupling on virtual impedance, under the condition of different charging voltages.

LS40K130QP, LS40K230QP, LS40K320QP, LS40K420QP and LS40K550QP coupling. Accordingly, the combination wave test level should exceed 3.3 kV/1.5 kA, 5.5 kV/2.5 kA, 6.4 kV/2.9 kA, 9.1 kV/4.2 kA, and 15.8 kV/7.2 kA, respectively. Varistor coupling is not suitable for the testing occasion where testing level is a relatively low, such as 6 kV/3 kA as specified in UL 1449, although it has much less strict requirements in waveform parameters.

IV. Discussion

The normal operating voltage of varistor should be lower than the maximum operating voltage, otherwise, the heat generated under alternating current would exceed the dissipation ability and lead to the failure of thermal equilibrium. IEC 61643-11 requires that the voltage of power-supply network need to be adjusted to the maximum operating voltage (i.e., 52~1500 kV) in the testing of combination wave. In order to limit the power-frequency current flow from the power-supply network into the CWG, the impedance of coupling network need to be far larger than the equivalent impedance of the CWG. Therefore, almost all the voltage of power-supply network will be applied to the coupling network. If the varistor coupling is used, the requirement for testing SPD is that its maximum operating voltage needs to be lower than that of the coupling varistor. For instance, LS40K130QP is not an ideal coupling element for SPD whose maximum operating voltage is 320 V.

From the standpoint of the working voltage ranges in power-supply network of combination wave testing, a higher maximum operating voltage of coupling varistors is expected. However, the higher the maximum operating voltage, the worse its coupling performance. If a varistor with a good performance but a low maximum operating voltage is selected, the working voltage of the power-supply network will have to be limited to a narrow range. Hence, varistor can be applied to the test level which require less strict for the parameters of combination waveform.

The circuit configuration of CWG model in Fig. 1 is referred to IEC 61000-4-5. Other values of parameters with the same circuit configuration [18]-[20], or even other circuit configurations [18], [21], [22] can also give the normalized waveforms and fictive impedance of the CWG. In order to evaluate how the results presented in Section III could be affected by different choices of component values and configurations for the CWG, an extensive number of simulations with other CWG models were also performed. Obtained results show that, although there may be slight differences in parameters of OCV and SCC waveforms generated by specified CWGs, similar variation trends can be found for waveform parameters and fictive impedance with variation of the charging voltage.

V. Summary

Compared with the condition without any coupling element, reversed oscillation occurs in the waveform of open-circuit voltage under varistor coupling. Moreover, the peak value of open-circuit voltage and short-circuit current, as well as the front time and the tail time will be decreased, whereas the virtual impedance will be increased. For the involved six kinds of varistor coupling, when the charging voltage of storage capacitor of the combination wave generator is larger than 3.2, 5.2, 6.5, 8.6, 11.8, and 16.2 kV, respectively, the waveforms of coupled open-circuit voltage can meet the requirements of IEC 61643-11. For varistor coupling, the parameters of waveforms can meet the standard requirements such as IEC 61643-11 in a relatively limit range of combination wave testing level.

The lower the maximum operating voltage of varistors, the slighter the influence of varistor coupling on the output characteristics of the combination wave generator, and hence, the better the coupling performance. The varistor which has a lower maximum operating voltage is easy to be influenced by the working voltage scope of power-supply network, and hence, its application is limited.

Compared with the capacitive coupling, varistor coupling contributes to preventing the power-frequency current flow from the power-supply network into the combination wave generator, but is limited substantially in aspects such as the coupling performance, the working voltage range of the power-supply network and the combination wave testing level. The varistor coupling recommended by ITU-T K.44 can be applied to the test level which has much less strict requirements for the combination waveform parameters.

References

[1] *IEEE Recommended Practice on Surge Testing for Equipment Connected to LV (1000 V and less) AC Power Circuits*, ANSI/IEEE Std. C62.45-2002.

[2] *IEEE guide on the surge environment in low-voltage (1000 V and less) ac power circuits*, ANSI/IEEE Std. C62.41.1-2002.

[3] *IEEE recommended practice on characterization of surges in low-voltage (1000 V and less) ac power circuits*, ANSI/IEEE Std. C62.41.2-2002.

[4] M. Zhou, J. Wang, Y. Liu, and F. Liu, "Coupling and Decoupling Network for Surge Immunity Test on Power Lines," in *Proc. 2008*

International Conference on Electrical Machines and Systems, 2008, pp. 151–155.

[5] M. Zhou, J. Wang, X. Fan, L. Cai, C. Fang, and J. Xue. "Influence of power-line coupling/decoupling network on output characteristics of the combination wave generator, " *IEEE Trans. Power Del.*, vol. 26, no. 4, pp. 2333–2341, 2011.

[6] *Low-voltage surge protective devices –Part 11: Surge protective devices connected to low-voltage power systems –Requirements and test methods*, IEC 61643-11-2011.

[7] *UL Standard for Safety for Surge Protective Devices*, ANSI/UL 1449-2009.

[8] *Electromagnetic compatibility (EMC)—Part 4-5: Testing and measurement techniques—Surge immunity test*, IEC Std. 61000-4-5-2014.

[9] *Low-voltage surge protective devices –Part 1: Surge protective devices connected to low-voltage power distribution systems – Requirements and tests*, IEC Std. 61643-1-2005.

[10] M. A. Uman. *The art and science of lightning protection*, Cambridge University Press, 2010.

[11] *Resistibility tests for telecommunication equipment exposed to overvoltages and overcurrents – Basic Recommendation*, ITU-T Recommendation. K.44 -2008.

[12] H. R. Philipp and L. M. Levinson. "Long time polarization currents in metal oxide varistors," *Journal of Applied Physics*, vol. 47, no. 7, pp. 3177–3181, 1976.

[13] S. Tominaga, K. Azumi, Y. Shibuya. "Protective Performance of Metal Oxide Surge Arrester Based on the Dynamic V-I Characteristics," *IEEE Trans. Power Appar. Sys.*, vol. PAS-98, no.6, pp.1860–1871, 1979.

[14] IEEE Working Group 3.4.11. "Modeling of metal oxide surge arresters". *IEEE Trans. Power* Del., vol. 7, no.1, pp. 302–309, 1992.

[15] P. Pinceti and M. Giannettoni. "A simplified model for zinc oxide surge arresters," *IEEE* Trans*. Power Del*., vol. 14, no. 2, pp. 393–398, 1999.

[16] W. Schmidt, J. Meppelink, B. Richter B. "Behaviour of MO-surge-arrester blocks to fast transients," *IEEE Trans. Power Del.*, vol. 4, no.1, pp. 292–300, 1989.

[17] A. Haddad, P. Naylor, I. A. Metwally. "An improved non-inductive impulse voltage measurement technique for ZnO surge arresters," *IEEE Trans. Power Del*., vol. 10, no. 2, pp. 778–785, 1995.

[18] V. Radulovic and S. Skuletic, "Influence of combination wave generator's current undershoot on overvoltage protective characteristics," *IEEE Trans. Power Del*., vol. 26, no. 1, pp. 152–160, Jan. 2011.

[19] J. He, Z. Yuan, J. Xu, S. Chen, J. Zou, and R. Zeng, "Evaluation of the effective protection distance of low-voltage SPD to equipment," *IEEE Trans. Power Del*., vol. 20, no. 1, pp. 123–130, Jan. 2005.

[20] J. He, Z. Yuan, S. Wang, J. Zou, S. Chen, and Z. Rong, "Effective protection distances of low-voltage SPD with different voltage protection levels," *IEEE Trans. Power Del.*, vol. 25, no. 1, pp. 187–195, Jan. 2010.

[21] N. K. Medora and A. Kusko, "An enhanced computer simulation model of the IEEE Std C62.41.2-2002 surge generator for simulated surge testing of electrical systems," in *Proc. IEEE Symp. Product Compliance Engineering*, 2007, pp. 1–8.

[22] G. I. Stelios, "Comparative Study of Metal Oxide Varistors (MOVs) for Failure Mode Identification," MSc. dissertation, Dept. Elect. Eng., College of Engineering, Univ. South Florida, Tampa, FL, 2004.